Putative PSAT1 Small Molecule Inhibitors Decrease Breast Cancer Cell Proliferation and Synergize with Anti-Estrogen Therapies

S. Madison Duff, Brian Clem, Ph.D.
Departments of Biochemistry & Molecular Genetics and the James Brown Cancer Center
University of Louisville School of Medicine

Abstract

Despite aggressive treatments, a significant proportion of individuals with estrogen-receptor-positive breast cancer relapse after becoming resistant to current therapies. Therefore, the investigation of combinatorial therapies that could re-sensitize these cancers is necessary to identify further treatment options for these patients. It has been previously demonstrated that phosphoserine aminotransferase (PSAT1) is up-regulated in ER+ endocrine-resistant and triple-negative breast cancer. Thus, the serine pathway may be necessary to protect resistant breast cancer cells from common therapeutic drugs, including anti-estrogens and cytotoxic agents. We hypothesize that specific targeting of PSAT1 in combination with common chemotherapeutic agents may prove beneficial in treating endocrine-resistant and triple-negative breast cancers. In silico modeling of PSAT1 identified several chemical compounds that may suppress PSAT1 activity. Further analysis revealed two molecules that exhibited inhibitory activity on recombinant PSAT1. We now examined the ability of these antagonists to decrease breast cancer cell proliferation, as well as their combinatorial effect with the anti-estrogens, Tamoxifen and Fulvestrant, and common cytotoxic chemotherapies, doxorubicin, cyclophosphamide, and paclitaxel. In LY2 ER+ endocrine-resistant and MDA-MB-468 TNBC cells, treatment with two of the putative PSAT1 inhibitors resulted in a dose-dependent inhibition of cell proliferation. Additionally, combinatorial therapy with either Tamoxifen or Fulvestrant led to a synergistic decrease in LY2 cell growth. Co-treatment with the cytotoxic chemotherapy agents did not yield any increase in suppression of MDA-MB-468 breast cancer cell growth. Our data suggest that targeting PSAT1 through small molecule inhibitors may have utility against breast cancer proliferation and may prove beneficial in combination with anti-estrogen therapies.

.

Introduction

- Phosphoserine aminotransferase 1 (PSAT1) catalyzes the second step within the serine biosynthetic pathway via conversion of 3-phosphohydroxypyruvate to 3-phosphoserine.
- Prior computational modeling analysis identified several putative PSAT1 inhibitors (Figure 1).
- Tamoxifen is a selective estrogen receptor modulator and fulvestrant is a pure anti-estrogen.
- Doxorubicin is a DNA intercalator and generator of free radicals.
- Cyclophosphamide is an alkylating agent that induces cell death..
- Paditaxel exhibits cytoxic activity in tumor cells.
- Analyzing the synergy of each chemotherapeutic drug with designated PSAT1 inhibitors could lead to proposition of new combinatorial drug strategies.

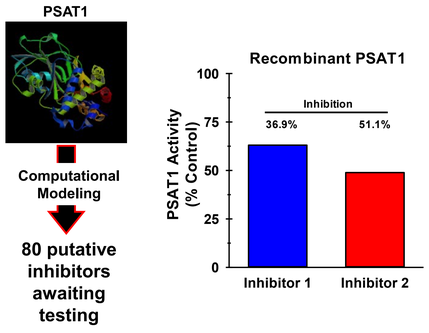

Figure 1. *In silico* identification of putative PSAT1 small molecule inhibitors.

Results

LY2: ER+ Endocrine Resistant Cells

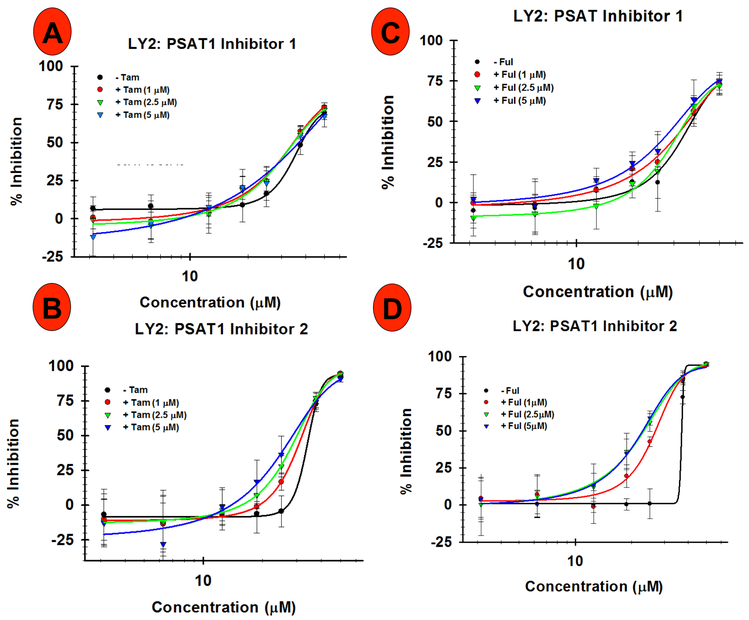

Figure 2. Effect of PSAT1 Inhibitors on Endocrine Resistant LY2 cells in combination with Tamoxifen or Fulvestrant. LY2 cells were treated with PSAT1 Inhibitor 1 (A & C) or PSAT2 Inhibitor 2 (B & D) with or without different concentrations of Tamoxifen (A & B) or Fulvestrant (C & D).

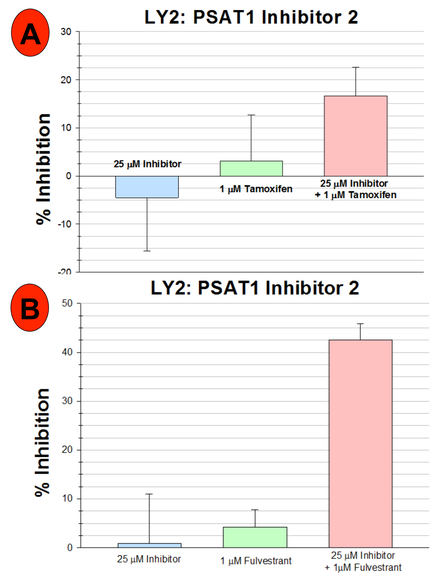

Figure 3. LY2 Growth Inhibition. LY2 cell growth at specific concentrations of PSAT1 Inhibitor 2 and Tamoxifen (A) or Fulvestrant (B).

MDA-MB-468: Triple Negative Cells

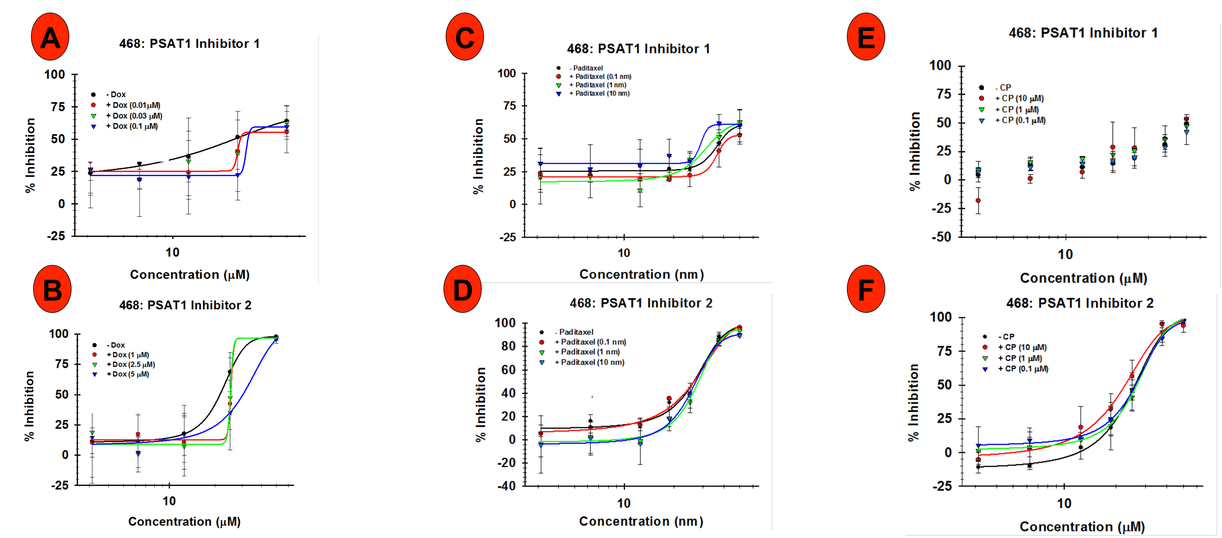

Figure 4. Effect of PSAT1 Inhibitors on Triple Negative 468 cells in combination with Doxorubicin, Paditaxel, or Cyclophosphamide. 468 cells were treated with PSAT1 Inhibitor 1 (A, C, & E) or PSAT2 Inhibitor 2 (B, D, & F) with or without different concentrations of Doxorubicin (A & B), Paditaxel (C & D), or Cyclophosphamide (E & F).

Methods

LY2 cells and MDA-MB-468 cells were plated in 250 μL of media in 48-well plates at experimentally determined densities, 5K and 10K per well respectively, and placed in an 37°C incubator to grow.

After 24 hours, the anti-estrogens, cytotoxic agents, and putative PSAT1 inhibitors were added in each well to bring the volume to 500 μL at final concentrations determined by previously published papers and/or experimental results.

After an additional 48 hours, cell growth was assessed in each well by means of the Sulfohodamine B Assay.

1) 250 μL of 50% TCA was added to the media in each well of the 48-well plate to fix the cells.
2) Plates were incubated for one hour at 4°C
3) Supernatant was discarded and each well was washed five times with tap water
4) The wells were let air dry and the remaining water was suctioned off 200 μL of Sulfohodamine in 1:1 acetic acid was added and left on for 10 minutes at room temperature
5) The wells were washed 5 times with 1% acetic acid to remove unbound dye and then given time to air dry
6) 250 μL of 10mM Tris sln was added to each well to solubilize the dye and the absorbance was read at 515 nm.

Conclusions

- Putative PSAT1 inhibitors 1 & 2 are effective in decreasing both ER+ and triple negative breast cancer cell proliferation in a dose-dependent manner.
- Both compounds appear to cooperate with the anti-estrogens tamoxifen and fulvestrant in reducing ER+ breast cancer cell growth.
- Combination of non-effective concentrations of PSAT1 inhibitor 2 and either anti-estrogen synergizes in suppressing proliferation of LY2 breast cancer cells.
- Addition of the clinically used cytotoxic agents, doxorubicin, paclitaxel, or cyclophosphamide, did not exhibit any additive effects in combination with the putative PSAT1 inhibitors against MDA-MB-231 triple negative cell growth.

Future Directions

- Correlate effects observed with these PSAT1 small molecule inhibitors to the effects of specific depletion of PSAT1 by siRNA mechanisms in order to determine potential off-target effects of the compounds on cell proliferation.
- Expand investigation into other cytotoxic agents, such as cisplatin or oxaliplatin.
- Examine additional putative PSAT1 inhibitors identified through computational screening on growth potential of breast cancer cells, including potential derivatives of inhibitors 1 & 2.

Acknowledgments

Research Supported by NIC R25 grant University of Louisville School of Medicine Cancer Education Program (NCI R25-CA134283).

Porphyromonas gingivalis induction of EMT transcriptional factors in gingival epithelial cells

R Gadde, M Sztukowska, RJ Lamont
University of Louisville School of Dentistry

Abstract

Objectives
To determine the effect *Porphyromonas gingivalis* (Pg) on transcriptional regulators of epithelial mesenchymal transition (EMT) in host epithelial cells.
Background
Oral Squamous Cell Carcinoma (OSCC) has 50,000 new cases and 13,500 deaths per year in the United States. EMT is a critical process in the growth of tumors. Oral bacteria are epidemiologically associated with OSCC tumors. Pg, an oral anaerobe, is consistently shown to be harbored at higher rates on tumor surfaces than normal gingiva. Pg also has been shown to impact expression of host genes related to apoptosis and cell cycle progression.
Hypothesis
Pg infection of epithelial cells will cause differential expression of EMT transcriptional regulators Zeb1, Zeb2 and Snail2.
Methods
The TIGK gingival epithelial line was infected with Pg at a multiplicity of infection (MOI) 10, 50, or 100 for various time points. RNA was extracted, and EMT transcriptional factors were quantitated with qRT-PCR. To show protein expression, cells were stained with antibodies for ZEB1 and examined by confocal microscopy. To assess the role of Pg fimbriae, TIGK cells were infected with a knockout strain defective in the gene encoding the major fimbrial protein of Pg (ΔfimA).
Results
Pg infection was shown to increase transcription of Zeb1, Zeb2 and Snail2 over a range of MOI and infection times. Pg infection also increased the amount of Zeb1 protein localized in the nucleus. When infected with the ΔfimA mutants TIGK cell expression of Zeb1, Zeb2 and Snail2 mRNA was significantly reduced compared to wild type Pg.
Conclusions
Pg increases expression of transcription factors that control EMT indicating that the organism could contribute to tumorigenesis in the oral cavity. FimA may have value as a potential therapeutic target and or biomarker.

Introduction

Oral and oropharyngeal cancers have over 50,000 new cases ever year and 13,500 deaths per year. Despite advanced therapeutic techniques, the 5-year survival rate for oral squamous cell carcinoma is estimated at 50%.
Previous studies have shown that oral bacteria can disrupt molecular pathways with relevance to cancer development and can enhance cancerous tumor growth. Oral bacteria are also epidemiologically associated with cancers such as pancreatic, colorectal, and oral squamous cell carcinoma (OSCC), and high levels of certain salivary bacteria have been shown to be possible indicators of OSCC. Moreover, OSCC surfaces harbor significantly higher levels of *Porphyromonas gingivalis* (Pg) compared with healthy mucosa, and immunohistochemistry with Pg antibodies revealed higher levels of staining in OSCC compared with healthy gingiva.
The goal of this project is to determine the effect of Pg on the epithelial-mesenchymal transition (EMT). Zeb1, Zeb2, and Snail2 are transcription factors which play an important role in controlling effectors and markers of the EMT. One of the major proteins that allows Pg to interact with and invade host cells is the major fimbrial protein A (FimA), and the role of FimA in the regulation of EMT transcription factors was investigated.

References

1 Caygill, C. P. Bacterial infection and human cancer: association or causation? Commun Dis Rep CDR Rev 2, R7-9 (1992).
2 Cronin, K. A., Ries, L. A. & Edwards, B. K. The Surveillance, Epidemiology, and End Results (SEER) Program of the National Cancer Institute. Cancer 120 Suppl 23, 3755-3757, doi:10.1002/cncr.29049 (2014).
3 Dave, N. et al. Functional cooperation between Snail1 and twist in the regulation of ZEB1 expression during epithelial to mesenchymal transition. J Biol Chem 286, 12024-12032, doi:10.1074/jbc.M110.168625 (2011).
4 Eke, P. I. et al. Prevalence of periodontitis in adults in the United States: 2009 and 2010. J Dent Res 91, 914-920, doi:10.1177/0022034512457373 (2012).
5 Farnebo, L. et al. Targeting Toll-like receptor 2 inhibits growth of head and neck squamous cell carcinoma. Oncotarget (2015).
6 Katz, J., Onate, M. D., Pauley, K. M., Bhattacharyya, I. & Cha, S. Presence of *Porphyromonas gingivalis* in gingival squamous cell carcinoma. Int J Oral Sci 3, 209-215, doi:10.4248/IJOS11075 (2011).
7 Krisanaprakornkit, S. & Iamaroon, A. Epithelial-mesenchymal transition in oral squamous cell carcinoma. ISRN Oncol 2012, 681469, doi:10.5402/2012/681469 (2012).
8 Lamouille, S., Xu, J. & Derynck, R. Molecular mechanisms of epithelial-mesenchymal transition. Nat Rev Mol Cell Biol 15, 178-196, doi:10.1038/nrm3758 (2014).
9 Lim, J. & Thiery, J. P. Epithelial-mesenchymal transitions: insights from development. Development 139, 3471-3486, doi:10.1242/dev.071209 (2012).
10 Lin, F.Y. et al. The GroEL protein of *Porphyromonas gingivalis* accelerates tumor growth by enhancing endothelial progenitor cell function and neovascularization. Mol Oral Microbiol, doi:10.1111/omi.12083 (2014).
11 Nagy, K. N., Sonkodi, I., Szoke, I., Nagy, E. & Newman, H. N. The microflora associated with human oral carcinomas. Oral Oncol 34, 304-308 (1998).
12 Nieto, M. A. The ins and outs of the epithelial to mesenchymal transition in health and disease. Annu Rev Cell Dev Biol 27, 347-376, doi:10.1146/annurev-cellbio-092910-154036 (2011).

Background

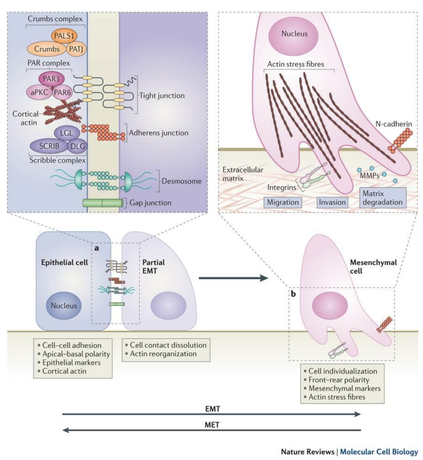

Epithelial Mesenchymal Transition is characterized by the loss of normal cell-cell adhesion and cell polarity. The cell matrix undergoes degradation which allows the cell to mobilize, causing metastasis. Figure taken from Lamouille et al (2014).

Methods

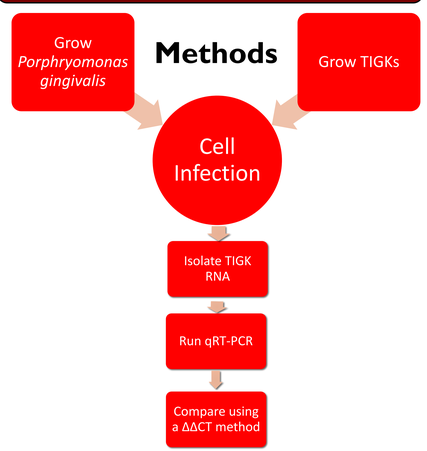

TIGKs and Pg were grown, the TIGKs were infected with the Pg and RNA was extracted for qPCR. The experiment was repeated with mutants and infections were done separately for confocal imaging. ANOVA or paired T-test were used to determine significance. * $p<0.05$ was considered significant. **, indicates $p<0.01$, *** or ### indicate $p<0.005$.

Results

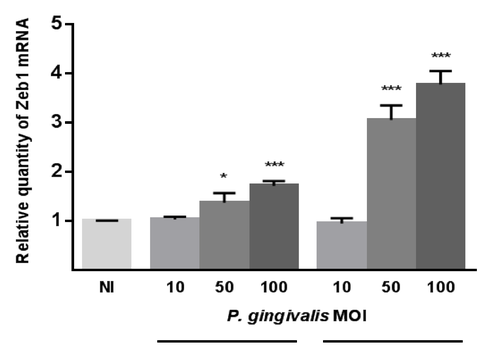

TIGKs infected with Pg wild type at MOI and times indicated showed increased ZEB1 expression. ZEB1 is a positive regulator of the EMT process.

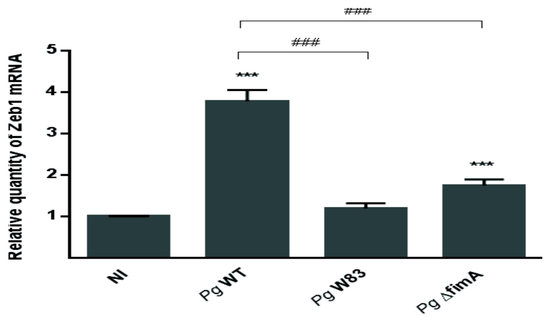

TIGKs infected with Pg wild type (WT) at MOI 100 for 24 h showed increased ZEB1 expression. In contrast, Pg strains lacking FimA naturally (W83) or as a result of gene disruption (ΔfimA) showed a diminished ability to upregulate ZEB1.

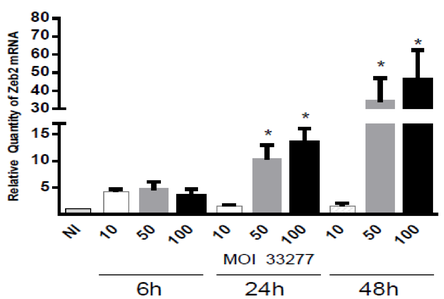

TIGKS infected with Pg at the times and MOI indicated show significant increase in ZEB2 expression.

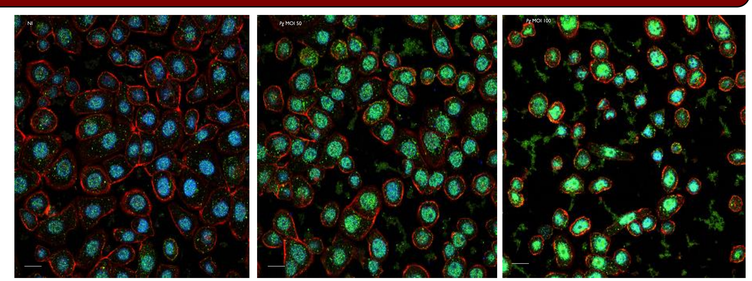

Fluorescent confocal microscopy of TIGK cells (stained with TITRC-phalloidin, red) infected with Pg confirmed increased expression of ZEB1 protein (stained with antibodies, green) in the nucleus (blue) where it is functionally active.

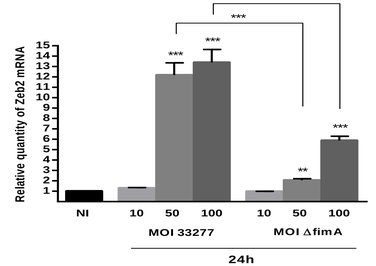

The Pg ΔfimA strain is less efficient than WT at upregulating Zeb2 mRNA levels.

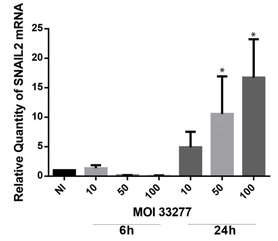

Over different MOIs of Pg, SNAIL2, another EMT transcription factor is upregulated

Conclusions

- **Infection of epithelial cells by Pg causes EMT transcriptional regulators to express at significantly higher levels.**
- **FimA significantly enhances *Pg* induced expression of ZEB1, ZEB2and SNAIL2.**
- **FimA, which is unique to Pg may have value as an early biomarker of OSCC or as a potential therapeutic target.**

Acknowledgments

Research supported by:
- University of Louisville
- National Cancer Institute grant R25-CA134283
- NIDCR grants DE011111, DE017921, DE012505, DE016690 and DE023193
- Lamont Lab members

Role of sphingosine kinase 1 and 2 in MYC-induced leukemogenesis

Alexandra Kiefer[1], Morgan Stathem[1], Michael Scherzer[1], Brian Wattenberg[1], Levi J Beverly[1], Leah J Siskind[1], and Deanna Siow[1]

[1]University of Louisville School of Medicine, Louisville, Kentucky

ABSTRACT

Sphingosine kinases (SKs) catalyze the conversion of sphingosine to sphingosine-1-phosphate (S1P), a lipid mediator of inflammation, cell proliferation, angiogenesis, and other pro-survival cellular processes. Altered levels of key sphingolipids have been observed in a wide variety of cancers; our lab is interested in the role of altered sphingolipid metabolism with regards to acute myeloid leukemia. Previously, our lab developed an *in vivo* screen in mice for identification of potential drivers of leukemia. Using this screen, we identified the two SK isoforms, SK1 and SK2, as cooperators with the oncogene MYC in the induction of leukemia. The long-term purpose of this project is to determine the specific domains within the SK proteins that are required for cooperation with MYC in the induction of leukemia. To this end, we created mutations in specific regions of the SKs, including the catalytic domains and phosphorylation sites. The impact that these mutations had on expression and activity was analyzed *in vitro* in HEK293 cells. Expression of WT and mutant forms of SK1 and SK2 were evaluated via real-time PCR and western analysis and compared to the enzymatic activities that were quantified using a radiolabeled assay. Now that our mutant forms of SK1 and SK2 have been characterized, future experiments will involve co-expressing them with MYC in our Tet-O-MYC mouse model of leukemia. Further characterizing the SK-MYC cooperation will provide an understanding of leukemogenesis mechanisms for identification of potential therapeutic targets. This research was supported by National Cancer Institute grant R25-CA134283.

BACKGROUND

Figure 1. Pathway showing the biosynthesis of sphingosine from ceramide. Its conversion to sphingosine-1-phosphate is then facilitated by sphingosine kinase. Altered sphingolipid metabolism has been observed in a wide variety of cancers, including AML. The translocation of SK may be necessary for its role in oncogenesis.

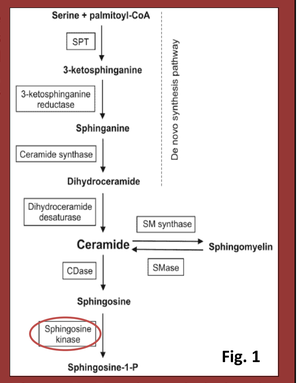

Fig. 1

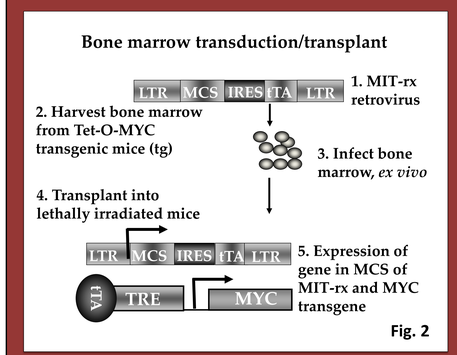

Fig. 2

Figure 2. Experimental design for testing the *in vivo* potential of genes (cloned into the multi-cloning site, MCS, of MIT-rx) in cooperating with MYC in leukemogenesis.

Figure 3. Our *in vivo* model shows that expression of SK1 and SK2 accelerates MYC-induced leukemia. BCLxl is shown as a positive control for a potent MYC cooperator, and GFP is shown as a negative control.

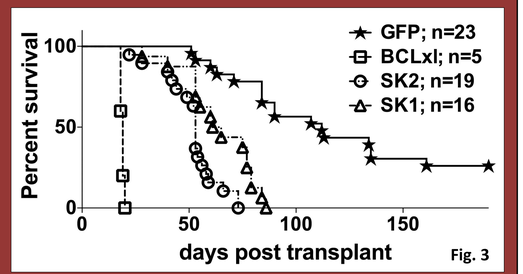

Fig. 3

METHODS

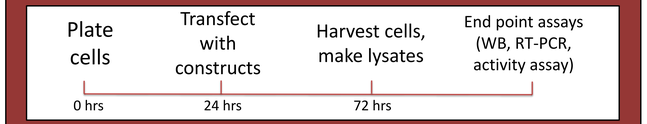

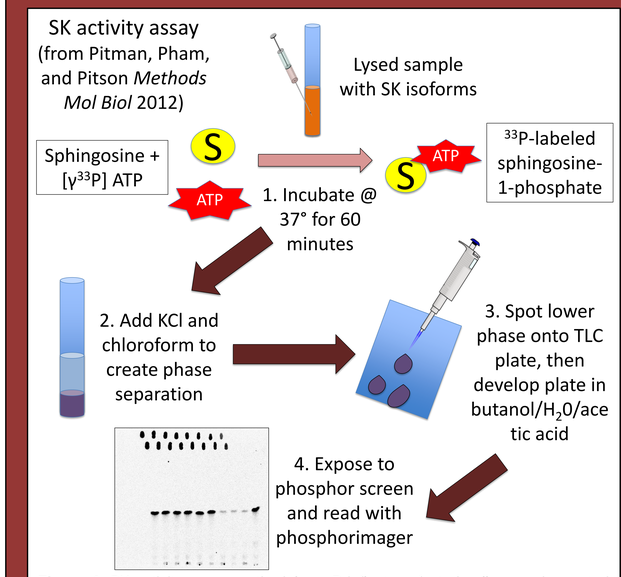

Figure 4. SK activity assay methodology. Briefly, transfected cells were harvested and cell pellets were lysed in buffers designed for optimal activity of each isoform using 10 passages through a 26G needle. Lysates were clarified by centrifugation at 10,000xg for 10 minutes at 4°C. Protein concentration was measured using Bradford assay and each reaction was carried out with 2.5ug total protein. SK activity was assessed by incubating lysates with reaction mixture (20mM Mg-ATP, 10uCi/uL [γ^{33}P] ATP, 2mM sphingosine in 5% Triton X-100 or 2% fatty acid-free BSA, 50mM 4-deoxypyridoxine, optimal assay buffer) at 37°C for 60 minutes (based on initial time course experiments). Reactions were quenched with 300uL chloroform/methanol/conc. HCl (100:200:1). Phases were separated using additional chloroform and KCl, after which samples were vortexed then centrifuged for 5 minutes at 13,000xg. Lower, organic phase was removed and 45uL of each sample was applied to prepared thin-layer chromatography (TLC) plates. TLC plates were developed with butanol/H2O/acetic acid (60:20:20, v/v) then allowed to dry prior to applying ATP standards and placing them on phosphor screens overnight. Images were obtaining using a BioRad PharosFX. Volume readings for each band were obtained and levels of radiolabeled S1P were quantitated based on known standards on each plate.

RESULTS

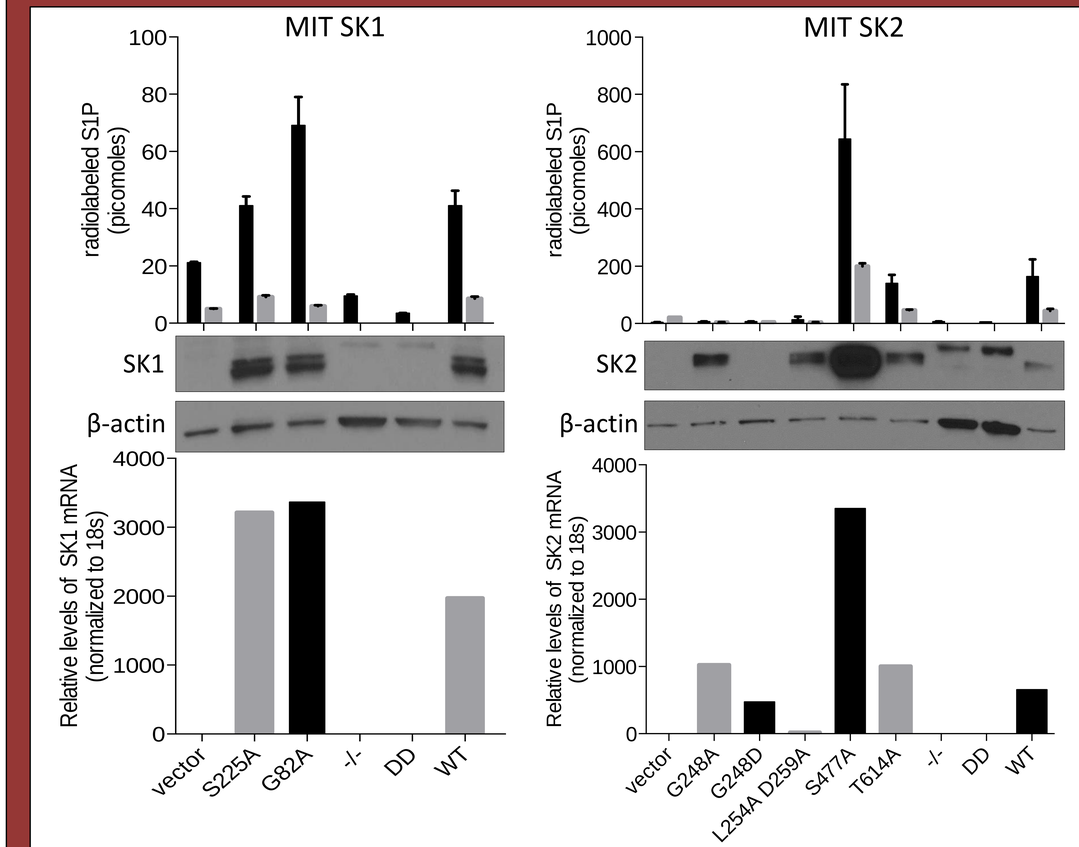

Figure 5. Results of the end point assays for SK1 (left) and SK2. SK activity assay (top): see methods section. Western blot (middle): 20ug of total protein per sample was loaded onto a BioRad 12-20% gradient gel. Proteins were transferred to a PVDF membrane then blocked with 5% milk in TBST. Membrane was incubated overnight in anti-SK antibody (gift of Binks Wattenberg, 1:1000 in TBST with 1% milk). Following HRP-tagged secondary antibody, proteins were imaged using ECL Prime reagent and exposed to film. RT-PCR (bottom): Cells were harvested with trypsin and total RNA was isolated using TRIzol and phase lock gels. cDNA was prepared using 1ug total RNA per sample, then 10ng cDNA was used for quantitative real-time PCR. TaqMan reagents were used for all real-time reactions and samples were normalized to levels of 18s.

CONCLUSIONS & FUTURE DIRECTIONS

We were able to characterize the relative expression and activity of our mutant SK1 and SK2 isoforms *in vitro*. With this quantification as a guide, future directions include:

- Co-expressing the wild type and mutant SK isoforms with MYC in our TET-O-MYC mouse model of leukemia
- Determining the specific domains that interact with MYC to potentiate leukemogenesis

ACKNOWLEDGEMENTS

This research was supported by the R25 University of Louisville Cancer Education Program (NCI grant R25-CA134283).

Small Dual Surfactant Mesoporous Silica Nanoparticles Demonstrate Acidic pH Specificity

Matthew S. Neal, Benjamin Fouts, Phillip Chuong, Alexander Sobolev, Molly McNally, Bigya Khanal, Anil Khanal, Lacey R. McNally

University of Louisville School of Medicine

Abstract

Localized delivery of drug and contrast agent has the potential to address the current inadequacies of pancreatic adenocarcinoma diagnosis and treatment. With a five-year survivability of 6%, this phenotype is the deadliest form of cancer. The poorly ordered vasculature of pancreatic tumors combined with the shortcomings of current imaging modalities make this disease difficult to diagnose and treat effectively. We created 25 nm, pH responsive, peptide targeted, mesoporous silica nanoparticles (MSNs) to act as a diagnostic nanodelivery system that preferentially delivers contrast to pancreatic tumors. The MSNs were conjugated with chitosan and V7 pH low insertion peptide to impart pH responsiveness and pancreatic tumor targeting, respectively. It was determined that loading the MSNs with IR 780 iodide dye did not appreciably alter the absorbance peak (dye: 780 nm; loaded dye: 804 nm), though signal attenuation was observed. Pancreatic cell lines Panc1 and S2VP10 were assessed for MSN binding at physiological pH (7.4) and at cancerous pH (6.6). It was found that the MSNs showed 45.6x the fluorescence at pH 6.6 that was seen at pH 7.4, confirming pH responsive cell binding. These findings suggest that this type of nanodelivery system is a good candidate for future use with *in vivo* models of pancreatic adenocarcinoma.

Methods

Synthesis: Mesoporous silica nanoparticles (MSNs) were synthesized using a dual surfactant method, with cetyl trimethylammonium chloride (CTAC, 3.6 g, 8.14 mmol) as the pore scaffolding and triblock copolymer Pluronic F127 (2.0 g, 0.159 mmol) as the growth limiting agent. Surfactants were dissolved in HCl solution (30 mL, pH 0.5), then tetraethyl orthosilicate (TEOS, 3.5 g, 16.8 mmol) was introduced to the solution at 4° C and stirred for 12 hours. The reaction was pushed to completion by adding ammonia water (3 mL, 14.7 M). A white gel formed and was aged for 24 hours. Sample was collected via centrifugation and washed in ethanol three times, then three more times in a solution of ethanol and ammonium nitrate (95% ethanol by volume, 5% ammonium nitrate by volume) to remove surfactants. Particles were dried in heated vacuum (60° C, 12 hr) and stored as a powder.

Chitosan Addition: Particles (0.1 g) were resuspended in ethanol (10 mL). To functionalize the MSN surfaces, (3-aminopropyl)triethoxysilane (APTES, 100 uL) was introduced into the resuspension and stirred for 12 hours. The functionalized particles were then mixed with a solution of acetic acid and chitosan (5% acetic acid by volume, 1% chitosan by weight) for 12 hours. The resultant C-MSNs were collected by centrifugation and washed in ethanol, and stored in an ethanol suspension.

Dye Loading: Suspended C-MSNs were mixed with a solution of IR 780 Iodide dye (3.3 mM) in dimethylformamide (DMF). This solution was acidified to pH 3 with HCl (5 M) and stirred for 24 hours to allow dye to equilibrate within the C-MSNs. The solution was then titrated to pH 7.4 with NaOH (5 M) to close the dye into the particles. Particles were dialyzed in 1:9, PBS:DI water solution for 4 hours to remove excess dye.

pHLIP Targeting: To add binding sites for the pHLIPS, APTES (30 uL) was added to the dye loaded C-MSNs and stirred for 1 hour. Succinimidyl 4-(N-maleimidomethyl) cyclohexane-1-carboxylate (SMCC, 30 uL)) was added to solution and stirred for 1 hour. Finally, the pHLIP (50 uL, 5 mM), dissolved in DMF, was introduced to the solution and stirred for 1 hour. Particles were dialyzed in 1:9 PBS to DI water and stored in suspension.

***In Vitro* Assay:** Two pancreatic cancer cell lines, Panc1 and S2VP10, were assessed for pH responsive uptake of pHLIP targeted C-MSNs. Cells were grown to confluence, then treated with pH specific media (pH 7.4 or 6.6) for 3 hours. Cells were then treated with targeted C-MSN solution and incubated for 10 minutes. Media was removed after incubation and cells were washed for 10 minutes with PBS (pH 7.4 or 6.6). After the wash, cells were imaged on the Licor Odyssey.

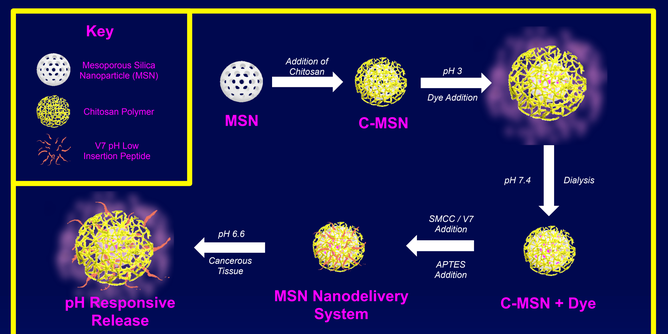

Figure 1: Synthesis of Nanodelivery System. *Mesoporous silica nanoparticles (MSNs) are incapable of retaining a deliverable payload without modification. The addition of chitosan ensures not only that the payload will be secure, but also that it will not be released until it is exposed to the pH of the cancerous target. Adding dye is similar to releasing dye, where a low pH causes conformational change in chitosan and allows dye to flow in or out of the MSN. When conjugated with the V7 pH low insertion peptide, MSNs will be preferentially phagocytized in acidic environments, allowing for a targeted nanodelivery system.*

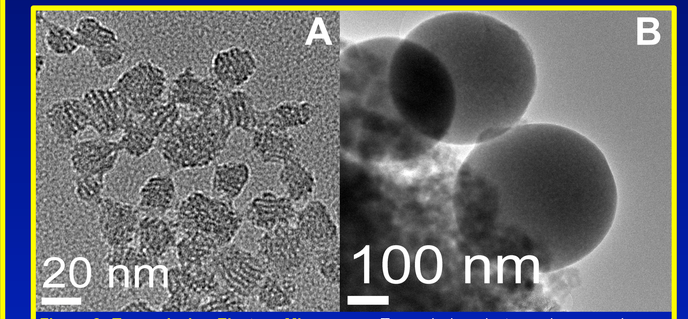

Figure 2: Transmission Electron Microscopy. *Transmission electron microscopy images showed that the synthesized mesoporous silica nanoparticles had a well-ordered structure with evenly spaced pores. The MSNs had an average diameter of 25 nm and a pore size of 2 nm. After chitosan coating, the C-MSNs (right) were spherically shaped with an average diameter of 280 nm. Microscopy confirmed the structure and shape of the nanoparticles after synthesis and coating.*

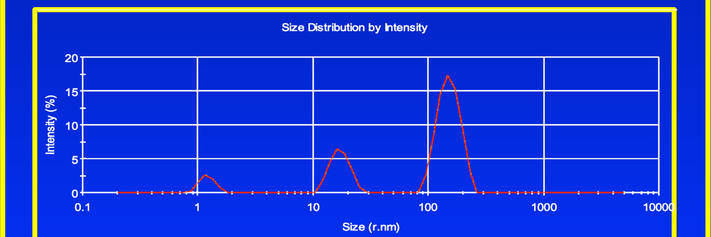

Figure 3: Dynamic Light Scattering. *Dynamic light scattering was implemented to determine if particle synthesis was successful. Readings showed particles at 2 nm in radius, 20 nm in radius, and 170 nm in radius. The 170 nm readings were thought to be accumulations of smaller particles due to the poor solubility of silicon dioxide in water.*

Results

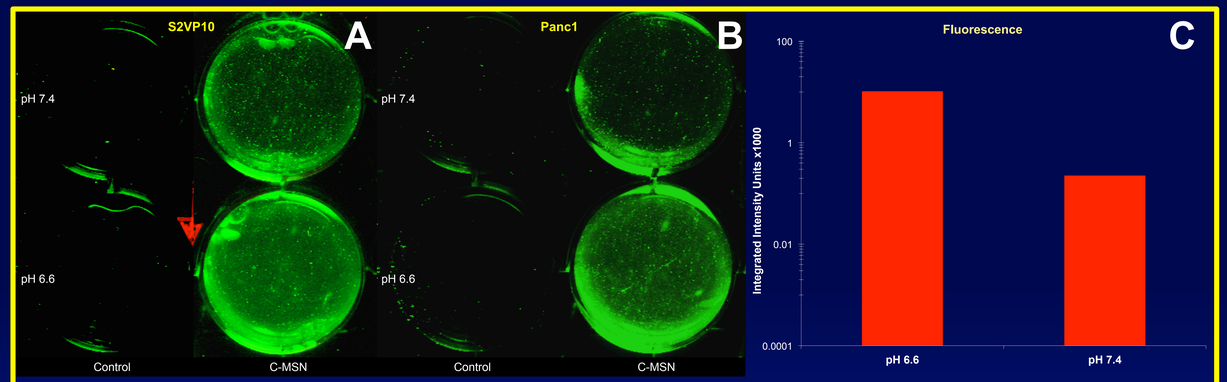

Figure 5: Cell Fluorescence Assay. *Pancreatic cancer cell line Panc1 were treated with dye loaded nanoparticles at pH 7.4 and pH 6.6 to determine preferential binding capacity of the mesoporous silica nanodelivery system (wells, left). Licor Odyssey imaging revealed a substantial difference in fluorescence between cells at physiological pH (7.4) and cells of cancerous pH (6.6), strongly suggesting that the mesoporous nanodelivery system shows preferential cellular uptake in acidic models of pancreatic adenocarcinoma. Acidic cells showed 45.6x the fluorescence of cells in physiological pH (chart, right). Controls were Panc1 cells that were untreated with nanoparticle, incubated in the both pH 7.4 and pH 6.6 media as the treated cells. This binding profile suggests effectiveness in vivo.*

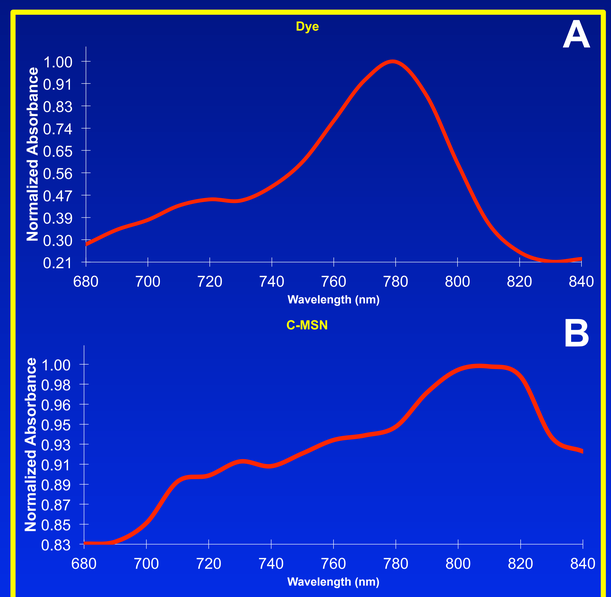

Figure 4: Absorbance Spectra. *Upon loading IR 780 Iodide into the MSNs it became necessary to asses the absorbance characteristics of the particles with dye compared to the dye itself. This analysis showed the effect the loading process had upon the fluorescence of the dye. It was determined that the dye (top) had a peak absorbance wavelength of 778 nm and the loaded MSNs had a peak absorbance wavelength of 804 nm. The loading process did not significantly alter the shape of the curve, but did attenuate the signal intensity.*

Conclusions

Well ordered, mesoporous silica nanoparticles, coated with chitosan, and targeted with pH low insertion peptides show promise as a means of controlled drug delivery *in vivo*.

In vitro trials with IR 780 Iodide show significant differences in fluorescence from nanoparticles that have an absorbance curve very similar to that of the unloaded dye.

A dual surfactant method of synthesis limits particle growth in a Stober nanoparticle growth process and allows for the creation of small mesoporous silica nanoparticles.

Future Studies

In the future, we would like to explore variable chitosan coating thicknesses for optimized contrast retention and release kinetics in mesoporous silica. We also plan to begin *in vivo* trials with mouse models, using Multispectral Optoacoustic Tomography as the primary imaging modality. This imaging modality will enable us to track *in vivo* dye release kinetics in real time without sacrificing the animal. This will allow for comparison with *in vitro* release kinetics and the potential to begin Gemcitabine trials *in vivo*. Future *in vivo* testing of these nanoparticles will move targeted theranostics one step closer to clinical translation.

Acknowledgements

Research supported by a grant from the NCI R25-CA134283 and the School of Medicine Cancer Education Program.

Genetic polymorphisms in 5-FU related enzymes predict complete pathologic response in rectal cancer

Bailey Nelson, B.S.[1], Jane Carter, MBChB[1], Maurice R. Eichenberger, M.S.[1], Uri Netz, M.D.[1], Susan Galandiuk, M.D.[1]
Digestive Surgery Research Laboratory, Price Institute of Surgical Research[1]
University of Louisville School of Medicine

Introduction

Patients with locally advanced rectal cancer undergo preoperative neoadjuvant chemoradiation with approximately 70% exhibiting pathologic downstaging in response to treatment. Of these, 15-20% of patients exhibit “complete pathologic response” with no remaining viable cancer. There is currently no accurate test to identify patients who are complete responders to neoadjuvant therapy who may be able to avoid undergoing radical surgery.

5-Fluorouracil (5-FU) is an antimetabolite drug that is widely used in the neoadjuvant treatment of rectal cancer. Genetic polymorphisms affect the activity of enzymes involved in 5-FU metabolism, such as thymidylate synthase (TYMS), and may also account for differing responses to neoadjuvant treatment seen in rectal cancer patients. Detection of such polymorphisms might permit identification of patients likely to have a complete response to neoadjuvant therapy.

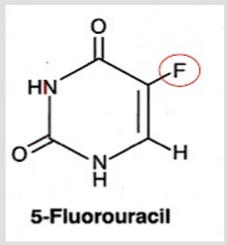

Figure 1. 5-FU Structure
5-FU is a pyrimidine analog that causes a halt in DNA replication and cancer cell death.

Methods

1. DNA was isolated from whole blood taken from patients with newly diagnosed rectal cancer who received neoadjuvant therapy (n=54) and whole genome amplification was performed.
2. Medical records were reviewed and a tumor regression grade (TRG) was given based on pre- and post-operative TNM staging (Ryan *et al*., 2005).

Description	Tumor Regression Grade
No viable cancer cells or single cells/small groups of cancer cells	1
Residual cancer outgrown by fibrosis	2
Significant fibrosis outgrown by cancer or no fibrosis with extensive residual cancer	3

3. Polymerase Chain Reaction (PCR) was performed using previously published primers targeting the promoter region of TYMS (Pullarkat *et al*., 2001).
   Forward: 5’-GTGGCTCCTGCGTTTCCCCC-3’
   Reverse: 5’-GCTCCGAGCCGGCCACAGGCATGGCGCGG-3’
4. PCR products were separated by electrophoresis on a 3% agarose gel to visualize if a patient was homozygous for a double-tandem repeat (2R), a triple-tandem repeat (3R), or heterozygous (2R/3R). A single nucleotide polymorphism (SNP) may also be present in the second repeat unit of the 3R allele.
5. Restriction fragment length polymorphism (RFLP) assays were performed on patients with at least one 3R allele using *HaeIII*, a restriction enzyme that recognizes the GGCC sequence and cleaves between the second and third nucleotides. The fragments were separated by electrophoresis.

Results

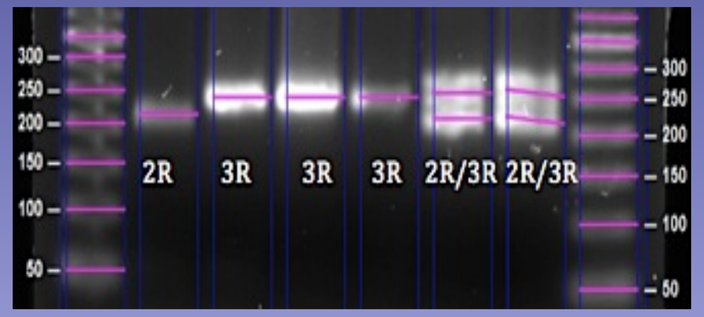

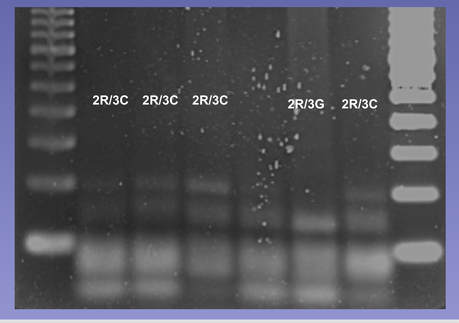

Figure 3 (*left*): **TS PCR Gel Electrophoresis**. The 2R allele band appears at 220-bp, while the 3R allele band appears at 250-bp.
Figure 4 (*right*): **RFLP Gel Electrophoresis**. SNPs were determined using a combination of PCR and RFLP gel electrophoresis results.

Genotype	2R/2R	2R/3R	3R/3R
# of patients	14	28	10

SNP	3C	3G
% of 3R population	26	20

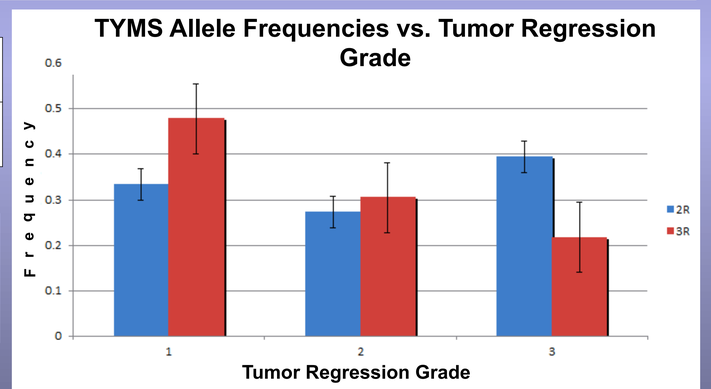

Figure 5 (left): **Frequency of TS Alleles and SNPs**.
Figure 6 (right): **TS Allele Frequency vs. TRG**. Patients with at least one TYMS 3G allele were more likely to have complete or partial pathological response to 5-FU neoadjuvant therapy (OR 9.6 95% CI 1.2 – 75.7) (p=0.02).

Conclusions

Identification of patients with specific genetic polymorphisms in enzymes involved in 5-FU metabolism appear to predict the likelihood of complete response of rectal cancer to preoperative 5-FU based neoadjuvant therapy and may alter surgical decision making.

Acknowledgements

Research supported by the National Cancer Institute grant R25-CA134283 and the John W. and Barbara Thruston Atwood Price Family Trust.

Combined Therapy of Oncolytic Adenovirus and Temozolomide Enhances Lung Cancer Virotherapy In Vitro and In Vivo

Jonathan Nitz[1] , Stephen L. Wechman[1], Eric Riedinger[1], Rajesh Sharma [2], Sam H. Zhou[1, 2], Kelly M. McMasters[1, 2] , Jorge G. Gomez-Gutierrez[1, 2]

[1]The Hiram C. Polk Jr., MD, Department of Surgery, and [2]The James Graham Brown Cancer Center
School of Medicine, University of Louisville

Introduction

•Lung cancer remains the leading cause of death from cancer worldwide. Most chemotherapy and molecular therapies are based on the induction of apoptosis. However, tumors frequently develop resistance to apoptosis prior to or during cancer treatment.

•Oncolytic adenoviruses (OAds) are very promising for the treatment of lung cancer. However, OAd-based monotherapeutics have not been effective during clinical trials. Therefore, the effectiveness of virotherapy must be enhanced by combining OAds with other therapies.

•In this study, the therapeutic potential of OAd in combination with temozolomide (TMZ) was evaluated in lung cancer cells *in vitro* and *in vivo*. The combination of OAd and TMZ therapy synergistically enhanced cancer cell death; this enhanced cancer cell death may be explained via three related mechanisms: apoptosis, virus replication, and autophagy. Autophagy inhibition partially protected cancer cells from this combined therapy. This combination significantly suppressed the growth of subcutaneous H441 lung cancer xenograft tumors in athymic nude mice.

•In this study, we have provided an experimental rationale to test OAds in combination with TMZ in a lung cancer clinical trial.

Results

1

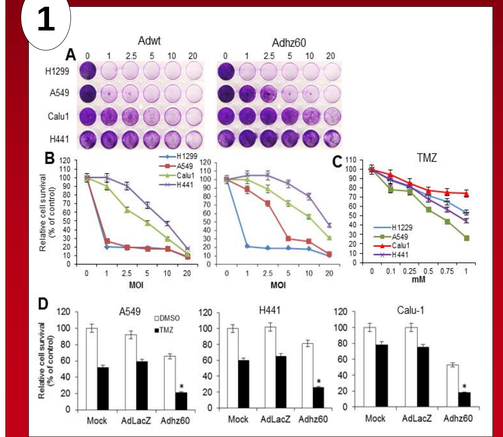

Fig. 1 Evaluation of oncolytic adenovirus-mediated cytopathic effect in permissive and non-permissive lung cancer cells and determination of TMZ IC_{50}

2

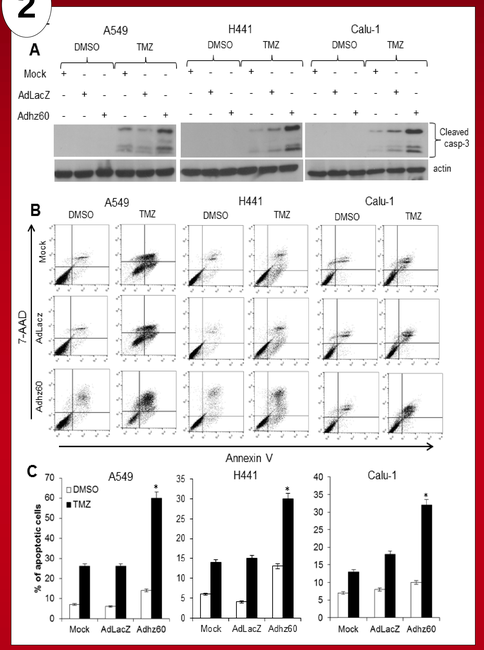

Fig. 2 Evaluation of apoptosis induction.

3

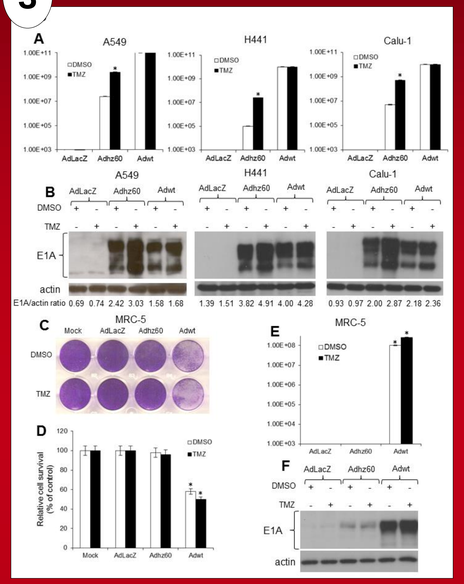

Fig. 3 Effect of TMZ on oncolytic adenovirus replication in permissive, non-permissive, and lung non-cancerous cells.

4

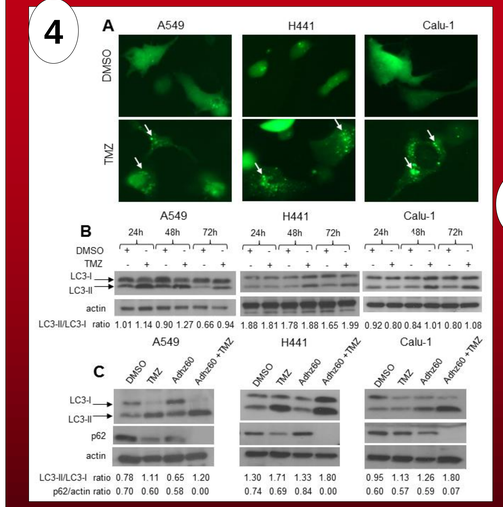

Fig. 4 Evaluation of TMZ ability to induce autophagy in lung cancer cells, enhanced autophagy using combination therapy, and the effect of autophagy inhibition using combined therapy-mediated cytotoxicity.

5

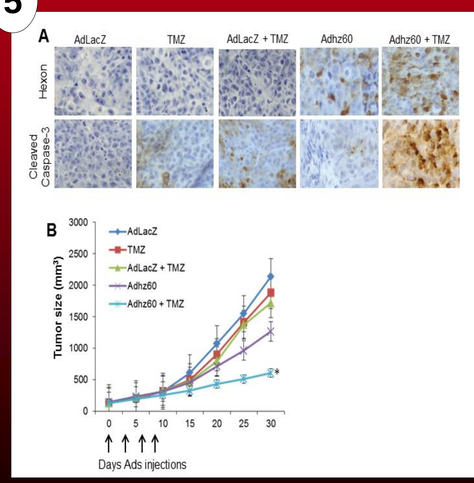

Fig. 5 Evaluation of the therapeutic potential of combined therapy of Adhz60 with TMZ in subcutaneous lung cancer mouse model.

Conclusions

In summary, TMZ-induced autophagy provides a better cellular environment for adenovirus replication. The combination of both TMZ and Adhz60 enhances their potency reciprocally. This study represents a potential alternative to lung cancer therapy, because the increased oncolytic adenovirus replication induced by TMZ may facilitate the virus spread within the lung tumors.

Acknowledgements

This work was supported by Award Numbers R01CA129975 (HSZ), R25-CA-134283 from the National Cancer Institute and Lung Cancer Research Fundation (JGGG).